Oral presentation | Turbulence simulation (DNS,LES,RANS)
Turbulence simulation(DNS,LES,RANS)-III
Thu. Jul 18, 2024 10:45 AM - 12:45 PM Room B

[10-B-02] Mode Analysis Using DNS Data of Oscillating Grid Turbulence Subjected to System Rotation

*Ryuga Sumi[1], Toru Yamada[1], Yohei Morinishi[1] (1. Nagoya Institute of Technology)

Keywords: DNS of Oscillating Grid Turbulence, Effect of System Rotation, Proper Orthogonal Decomposition, Dynamic Mode Decomposition

**Twelfth International Conference on
Computational Fluid Dynamics (ICCFD12),
Kobe, Japan, July 14-19, 2024**

Mode Analysis Using DNS Data of Oscillating Grid Turbulence Subjected to System Rotation

R. Sumi*, T. Yamada, and Y.Morinishi
Corresponding author: r.sumi.505@stn.nitech.ac.jp *
Graduate School of Engineering, Nagoya Institute of Technology,
Gokiso-cho, Showa-ku, Nagoya 466-8555, Japan.

Abstract: Turbulence subjected to system rotation provides significant insights into real-world flow phenomena, such as atmospheric and oceanic flows on Earth, and flow inside fluid machinery. Therefore, from the perspective of global environmental issues and energy efficiency in fluid machinery, it is indispensable to better understand the effects of rotation on turbulence. In order to investigate the effect of rotation on turbulence diffusion under the other effects being eliminated, this study performs a set of DNS of oscillating grid turbulence in systems at rest and with rotation. Also, two mode analysis methods, Proper Orthogonal Decomposition (POD) and Dynamic Mode Decomposition (DMD) methods, are applied to the velocity data to extract dominating flow structures. The results of the mode analyses show that the flow structures extracted are mainly categorized into the following three types regardless of the existence of system rotation: Large vortex structures, jet-like structures, and turbulence diffusion structures. The effects of rotation are found in the power spectral density in the POD result and the rank of the DMD modes ordered by the greedy algorithm.

Keywords: DNS of Oscillating Grid Turbulence, Effect of System Rotation, Proper Orthogonal Decomposition, Dynamic Mode Decomposition.

1 Introduction

Turbulence subjected to system rotation provides significant insights into real-world flow phenomena, such as atmospheric and oceanic flow influenced by the Earth's rotation and revolution, and flows inside fluid machinery like oil pumps and turbines. Therefore, from the perspective of global environmental issues and energy conservation in fluid machinery, it is indispensable to better understand the effects of rotation on turbulence.

To distinctly clarify the effects of rotation on turbulence, studying grid turbulence is effective, because shear free flow field on average can be achieved. There are two types of grid turbulence: one is the grid through turbulence where turbulence is generated by the flow passing through a stationary grid, where turbulence dissipation is predominant [1], and the another is the oscillating grid turbulence (OGT) where turbulence is generated by a grid oscillating in a stationary fluid, where turbulence diffusion is predominant [2][3]. This study focuses on the latter, i.e., OGT, to investigate the effect of rotation on turbulence diffusion under the other effects being eliminated.

In this study, we apply two mode analysis methods to the velocity fields obtained from Direct Numerical Simulations (DNS) in the systems at rest and subjected to rotation in order to analyze the flow structures of these flows. The DNS is a method that solves the governing equations directly without modeling the contributions of turbulence, allowing us to obtain velocity and pressure values. Unlike experiments,where secondary flows often arise due to effects such as walls of reservoir, DNS can realize an ideal flow field without secondary flows.

Previous studies on oscillating grid turbulence include both numerical [4] and experimental [2][3][5] studies, where the effects of rotation have been investigated through flow visualization and estimated turbulence statistics. These studies have ideal flow fields and analyzed turbulence statistics on the effects of rotation. In our previous experiment [6], the effects of low rotation rates were considered based on the turbulence statistics. However, detailed flow structures on the rotating system have not discussed in detail yet.

In the present study, we introduce mode decomposition methods to extract predominant spatial and temporal structures of the rotating turbulence from DNS data. For the mode decompositions, we introduce Proper Orthogonal Decomposition (POD) and Dynamic Mode Decomposition (DMD). The

POD identifies spatially orthogonal modes to capture the flow structures having larger energy, whereas the DMD decomposes the flow into modes having distinct frequencies and grow rates. By using these methods, the present study identifies the primary flow structures and the effects of rotation on them.

The rest of the present paper is organized as follows. In section 2, we provide an overview of the computational methods and mode decomposition techniques. The computational and analytical conditions are described in section 3. The results of the mode analysis of the OGT and the effects of rotation are presented in section 4. Finally, the present study is summarized in section 5.

2 Methodology

2.1 Numerical Simulation

In the rotating and translating acceleration coordinate system, the dimensionless continuity and the Navier-Stokes equations for an incompressible fluid (constant density ρ) are expressed as follows:

$$\frac{\partial u_j^\dagger}{\partial x_j^\dagger} = 0 \ , \tag{1}$$

$$\frac{\partial u_i^\dagger}{\partial t^\dagger} + \frac{\partial u_j^\dagger u_i^\dagger}{\partial x_j^\dagger} = -\frac{\partial P^\dagger}{\partial x_i^\dagger} + \frac{1}{Re}\frac{\partial}{\partial x_j^\dagger}\left(\frac{\partial u_i^\dagger}{\partial x_j^\dagger} + \frac{\partial u_j^\dagger}{\partial x_i^\dagger}\right) - \varepsilon_{i3k}\frac{1}{Ro}u_k^\dagger - \frac{d^2 y_i^\dagger}{dt^{\dagger 2}} \tag{2}$$

Here, quantities with superscript † are non-dimentionalized by using the characteristic length M and frequency f_g as follows:

$$x_i^\dagger = \frac{x_i}{M} \ , \ y_i^\dagger = \frac{y_i}{M} \ , \ u_i^\dagger = \frac{u_i}{M f_g} \ , \ t^\dagger = t f_g \ , \tag{3}$$

where x_i is the coordinate of the non-inertial frame, y_i is the x_i component of vector $\boldsymbol{y}$ which is the position vector from the inertial to the moving frames, t is time, and u_i is the velocity component of the x_i direction. Additionally, Re, Ro, and $P^\dagger$ are the Reynolds number, Rossby number, and dimensionless modified pressure, respectively, defined as follows:

$$Re \equiv \frac{f_g M^2}{\nu} \ , Ro \equiv \frac{f_g}{2\Omega} \ , P^\dagger \equiv \frac{p}{\rho M^2 f_g^2} - \frac{1}{2}\left(\varepsilon_{i3k}\frac{r_k^\dagger}{2Ro}\right)\left(\varepsilon_{i3l}\frac{r_l^\dagger}{2Ro}\right) \ , \tag{4}$$

where Ω is the system rotation around the x_3 axis, and P is pressure. In this study, we used a second-order finite difference method for the spatial discretization and a 2N-storage three-stage third-order Runge-Kutta method [7] for the time discretization. The corresponding pressure Poisson equation in this study is generated based on SMAC method [8]. For the details of solving the Poisson equation, refer to Ref. [9].

2.2 Mode Analysis

2.2.1 Proper Orthogonal Decomposition (POD)

In this subsection, we will briefly explain the mode analysis methods employed in this study: POD and DMD. POD [10] is a decomposition method that focuses on the variance of data, and it extracts low-dimensional components from high-dimensional data. It provides an orthogonal basis that represents the data most efficiently. By discretizing space and time, we prepare a column vector $\boldsymbol{x}(t_m) \in \mathbb{R}^{N_g}$ containing data from all spatial grid points at a certain time $t_m (m = 1, 2, \cdots N_t)$, where N_g is the total number of spatial grid points. These vectors are then compiled into a matrix $\boldsymbol{X}$ as follows:

$$\boldsymbol{X} = [\boldsymbol{x}_1, \boldsymbol{x}_2, \cdots, \boldsymbol{x}_{N_t}] \in \mathbb{R}^{N_g \times N_t} \tag{5}$$

At this point, the covariance matrix $\boldsymbol{R}$ of the data can be defined as follows:

$$\boldsymbol{R} = \boldsymbol{X}\boldsymbol{X}^T \tag{6}$$

The eigenvalues of the matrix $\boldsymbol{R}$ correspond to the variance when the data is projected onto the direction of the corresponding eigenvectors. The greater the variance, the more the data depends on that eigen-

vector. Therefore, by adopting the eigenvectors corresponding to the largest eigenvalues as the basis, the data can be represented most efficiently. This basis is called the POD modes. Additionally, if the POD modes are set as unit vectors, the dimension of the data is determined by the eigenvalues. If $\boldsymbol{x}(t_m)$ is velocity data, then the eigenvalues represent the energy of each mode. Since POD determines the POD modes based on the magnitude of the eigenvalues, the number of POD mode corresponds to the ranking of the energy contained in each POD mode.

In POD, eigenvalue decomposition is performed on the matrix $\boldsymbol{R} \in \mathbb{R}^{N_g \times N_g}$ to extract POD modes. This makes the computational cost extremely high because of a large number of spatial grid point, N_g. Therefore, in this study, we adopted Snapshot POD, which is improved to reduce the computational load. Snapshot POD computes the POD modes by performing eigenvalue decomposition on the smaller matrix $\boldsymbol{X}^T\boldsymbol{X} \in \mathbb{R}^{N_t \times N_t}$ instead of the matrix $\boldsymbol{R}$. Since N_t is the number of time points and in most cases $N_t \ll N_g$, the computational cost can be significantly reduced. The eigenvalues of the matrix $\boldsymbol{X}^T\boldsymbol{X}$ are the same as the eigenvalues μ_n^{POD} of the matrix $\boldsymbol{R}$. The POD modes ($\boldsymbol{\phi}_n^{\mathrm{POD}}$) can be calculated from the eigenvectors ($\boldsymbol{\psi}_n^{\mathrm{POD}}$) of the matrix $\boldsymbol{X}^T\boldsymbol{X}$ as follows:

$$\boldsymbol{\phi}_n^{\mathrm{POD}} = \frac{\boldsymbol{X}\boldsymbol{\psi}_n^{\mathrm{POD}}}{\sqrt{\mu_n^{\mathrm{POD}}}} \tag{7}$$

Furthermore, the Snapshot POD modes ($\boldsymbol{\psi}_n^{\mathrm{POD}}$) include the temporal information of the corresponding POD modes. The components of $\boldsymbol{\psi}_n^{\mathrm{POD}}$ correspond to the amplitudes of the POD modes at each discrete time point. Therefore, by performing Fourier analysis on $\boldsymbol{\psi}_n^{\mathrm{POD}}$, the frequency characteristics of the POD modes can be investigated.

POD can also be described using Singular Value Decomposition (SVD). The SVD of the matrix $\boldsymbol{X}$ is defined as follows:

$$\boldsymbol{X} = \boldsymbol{\Phi}\boldsymbol{\Sigma}\boldsymbol{\Psi}^T \tag{8}$$

Here, $\boldsymbol{\Phi}$ and $\boldsymbol{\Psi}$ are orthogonal matrices containing the eigenvectors of $\boldsymbol{X}\boldsymbol{X}^T$ and $\boldsymbol{X}^T\boldsymbol{X}$ respectively, i.e., $\boldsymbol{\phi}_n^{\mathrm{POD}}$ and $\boldsymbol{\psi}_n^{\mathrm{POD}}$ as columns. Additionally, $\boldsymbol{\Sigma}$ is a diagonal matrix with singular values, defined as the positive square roots of the eigenvalues of $\boldsymbol{X}\boldsymbol{X}^T$ and $\boldsymbol{X}^T\boldsymbol{X}$, i.e., μ_n^{POD}, as diagonal elements. Thus, it is understood that POD modes can also be obtained by SVD.

2.2.2 Dynamic mode Decomposition (DMD)

DMD[10] is a decomposition method that includes dynamic information from multidimensional data, yielding bases with intrinsic frequencies. By discretizing space and time, we convert the data at a spatial grid point at a certain time $t_m (m = 0, 1, \cdots N_t)$ into a column vector $\boldsymbol{x}(t_m) \in \mathbb{R}^{N_g}$, where N_g is the total number of spatial grid points. In DMD, it is assumed that the following linear relationship with the square matrix $\boldsymbol{A}$ holds:

$$\boldsymbol{x}(t_{m+1}) = \boldsymbol{A}\boldsymbol{x}(t_m) \tag{9}$$

Here, $\boldsymbol{A}$ is a square matrix. Expressed in matrix form, using the data matrices $\boldsymbol{X}_0 = [\boldsymbol{x}(t_0), \boldsymbol{x}(t_1), \cdots, \boldsymbol{x}(t_{N_t-1})]$ and $\boldsymbol{X}_1 = [\boldsymbol{x}(t_1), \boldsymbol{x}(t_2), \cdots, \boldsymbol{x}(t_{N_t})]$, we get the following equation:

$$\boldsymbol{X}_1 = \boldsymbol{A}\boldsymbol{X}_0 \tag{10}$$

The matrix $\boldsymbol{A}$ that satisfies equation (10) does not always exist. Therefore, matrix $\boldsymbol{A}$ is redefined by the following equation using the least squares method, and we choose the matrix $\boldsymbol{A}$ that is globally optimal. Here, the norm in the following equation is the Frobenius norm.

$$\underset{\boldsymbol{A}}{\mathrm{minimize}} \|\boldsymbol{X}_1 - \boldsymbol{A}\boldsymbol{X}_0\|_2^2 \tag{11}$$

At this time, using the eigenvalues (μ_n^{DMD}) and eigenvectors ($\boldsymbol{\phi}_n^{\mathrm{DMD}}$) of the matrix $\boldsymbol{A}$, the data $\boldsymbol{x}(t_m)$ is expressed as follows:

$$\boldsymbol{x}(t_m) = \sum_{n=1}^{N_g} \alpha_n (\mu_n^{\mathrm{DMD}})^m \boldsymbol{\phi}_n^{\mathrm{DMD}}, (m = 0, 1, \cdots, N_{\mathrm{time}}) \tag{12}$$

Here, α_n is a coefficient that arises during decomposition, indicating the initial amplitude and initial phase. If the eigenvectors are chosen as unit vectors, the information regarding the dimensions is ag-

gregated into α_n. This equation indicates that the data is represented using the eigenvectors of the matrix $\boldsymbol{A}$ as a basis. This basis is called the DMD mode. Additionally, information on the temporal evolution is obtained from the eigenvalues, and the Growth rate σ_n^{DMD} and frequency f_n^{DMD} of each mode are expressed as fellows:

$$\sigma_n^{\mathrm{DMD}} = |\mu_n^{\mathrm{DMD}}| \ , \tag{13}$$

$$f_n^{\mathrm{DMD}} = \frac{\mathrm{Arg}(\mu_n^{\mathrm{DMD}})}{2\pi\Delta t} \tag{14}$$

In this study, we conduct DMD analysis using an approximate solution method [11] that reduces computational cost by projecting the matrix $\boldsymbol{A}$ onto a smaller-sized matrix.

Unlike POD, where the eigenvalues directly correspond to the contribution to the data, several methods for ranking multiple modes have been proposed in DMD. In this study, we adopted the mode selection method based on the greedy algorithm [12]. This is an approximation method for combination optimization problems, defining an evaluation function and selecting in order of highest evaluation. The evaluation function in this study was the reconstruction error of each DMD mode.

3 Computational Setup

Figure 1 shows the model of the OGT for DNS and mode analysis. The computational domain is set to $4M \times 4M$ in the horizontal direction and $40M$ in the vertical direction, with the characteristic length being the grid mesh size M. The number of computational grids within this domain is 200×200 in the horizontal direction and 1400 in the vertical direction. The grid spacing is uniform in the horizontal directions (x_1, x_2) and in the vertical direction (x_3) within the region of the oscillating grid and the $10M$ region above and below the oscillation center. In other regions, to neglect the influence of grid oscillation at distant boundaries, a non-uniform grid expanded toward the upper and lower end faces using a tanh growth function is used. The grid rod width is $d = M/5$, and the grid oscillation stroke is $S/M = 6/5$. The grid oscillation is given by $y_3 = 0.5S\sin(2\pi f_g t + \theta_0)$ with an initial phase of $\theta_0 = -\pi/2$. The dimensionless time step is $f_g\Delta t = 1.25 \times 10^{-3}$ for the stationary system and $f_g\Delta t = 6.25 \times 10^{-4}$ for the rotating system. The Reynolds number is set to $Re = 5000$. These computational conditions correspond to a grid mesh size $M = 50$ mm, an oscillation stroke $S = 60$ mm, and a grid oscillation frequency $f_g = 2$ Hz. The boundary conditions for the flow field are no-slip on the oscillating grid surfaces, periodic boundary conditions in the horizontal direction, and a vertical velocity of $-S\pi\cos(2\pi t + \theta_0)$ set at the upper and lower end faces due to the oscillating grid being the origin of the rotating and translational acceleration coordinate system. In the rotating case, the system rotates around the x_3 axis with angular velocity Ω. In this study, $\Omega =$ 2 rpm is given, corresponding to a Rossby number of $Ro = 4.77$ as defined by Eq.(4). In the system at rest, $Ro = \infty$.

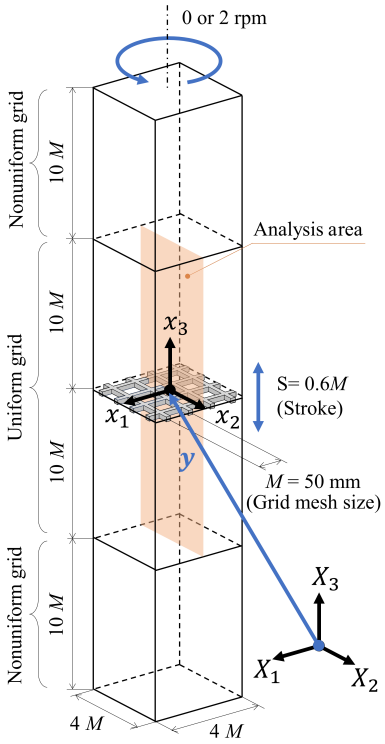

Figure 1 Computational domain. The orange-color plane is the section used for the POD and DMD analyses

The analysis region for mode analysis is the cross-section shown in orange-color in Figure 1. The input data for mode analysis is the velocity field data within the analysis region. However, the data inside the oscillating grid rods is the velocity of the oscillating grid. The discretization of the input data is the same as the DNS in the spatial direction, and in the temporal direction, it is divided into 40 parts (sampling frequency of $40f_g$) per oscillation of the grid, with a total of 400 points for 10 continuous periods. The coordinate system is an absolute coordinate system for the case at rest and a rotating coordinate system for the rotating case.

4 Results and Discussion

4.1 POD Modes for the System at Rest

In this subsection, we discuss representative POD modes among those extracted from the DNS results in the system at rest. The extracted structures are mainly categorized into following three types: 1) large vortex structures, 2) structures ejecting from the oscillating grid, and 3) turbulence diffusion structures. The structure types 1, 2, and 3 are shown in Figures 2, 3, and 4, respectively, of which the corresponding POD modes are the modes 1, 2, and 5. In each figure, (a), (b), and (c) show the power spectral density (PSD), the absolute value of velocity contours, and the streamlines, respectively.

First of all, the result of the large vortex structure, i.e., the POD mode 1 (Figure 2), is discussed. From Figure 2(a), it is observed that the PSD of this flow structure has peaks at the frequencies of integer multiples of f_g. Also, from Figure 2(b), large velocity region exist in the vicinity of the oscillating grid rods. On the other hand, in the region away from the oscillating grid, about $x_3/M > 0.5$, the velocity seems to be very small. Furthermore, from Figure 2(c), vertically stretched vortex structures having approximately one grid mesh size are observed on both sides of the grid rod, while in the region at $x_3/M > 0.5$, no distinct structures are observed. Although not shown here, there are several POD modes, similar to the POD mode 1, capturing flow structures with vortices in the vicinity of the oscillating grid and fluctuating with integer multiples of f_g. It is observed from these results that, for the dominant temporal frequency of the structure with $n \times f_g$, the number of vortices appearing on both sides of the grid rod are $2n$. This trend can also be observed in the DMD analysis as shown in the subsequent section.

Next, the structure extracted as the POD mode 2 (Figure 3) is discussed. From Figure 3(a), it is shown that the PSD at zero frequency is the most prominent, meaning that this structure consistenly exists in the flow field. There are also smaller peaks seen at the frequencies having integer multiples of f_g. From Figure 3(b), it is observed that, unlike POD mode 1, a large-velocity region exists in $x_3/M < 1$, which decays to the region of $x_3/M > 3$. From Figure 3(c), a jet-like flow structure ejecting the space in between the grid rods is observed. In summary, this POD mode appears to extract a structure stemming from the grid's oscillations, representing a steady ejection structure from space in between the grid rods to the far field. This ejection structure is presumed to be a jet-like flow from the space in between the oscillating grid rods to the far field.

Finally, the structure extracted as the POD mode 5 (Figure 4) is discussed. From Figure 4(a), it can be observed that the PSD for $f < 2f_g$ is prominent. This suggests that low-frequency oscillations are significant in this mode. Figure 4(b) shows that the velocity decays as it moves from the oscillating grid to the region away from the grid, approximately up to $x_3/M > 4$. It is probably due to the loss of energy as they move away from the grid. In Figure 4(c), no large-scale flow structure are evident, instead, the mode consists only of small-scale vortex structures. These observetions suggest that this mode primarily captures the turbulence diffusion structures.

Figure 5 shows the energy rate of the POD modes and its cumulative proportion. From the cumulative proportion, it is clearly shown that the top 10 POD modes represent about 60% of the original flow field. In terms of the energy rate for for each mode, it is observed that the energy rate drops to almost zero around the POD mode 5. This indicates that the POD modes larger than 5 contribute very little to the overall flow field.

Figure 6 shows the PSD of the POD modes from 1 to 100. It can be observed from the figure that the PSD has large peaks at the integer multiples of f_g. These are considered to be the frequencies for the vortex structures as demonstrated in Figure 2. These structures are considered to be excited by the oscillating grid and thus to be key energy sourses for turbulence diffusion. Also, for the modes without integer multiples of f_g representing the turbulence diffusion structures, the highly ordered ones have the peaks of the PSD at smaller frequences. This is because smaller frequencies generally have higher energy.

4.2 DMD modes for the System at Rest

In this subsection, we discuss representative DMD modes among those extracted from the DNS results in the system at rest. The extracted structures are categorized into the same three types as the ones extracted by the POD method. The structure types 1, 2, and 3 are shown in Figures 7, 8, and 9, respectively, of which the corresponding DMD modes are the modes 1, 2, and 5. For these figures, (a) and (b) show the absolute value of velocity contours and the streamlines, respectively.

First of all, the result of the large-scale vortex structure, i.e., the DMD mode 1 (Figure 7), is discussed. This mode has the frequency f_g. From Figure 7(a), large velocity regions exist in the vicinity of the oscillating grid rods. On the other hand, in the region away from the oscillating grid, $x_3/M > 0.5$, the

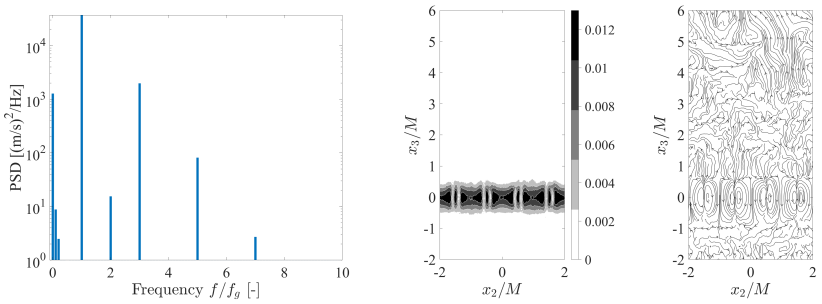

Figure 2 (a) Power spectrum density, (b) contour of velocity magnitude, and (c) streamlines for the flow structure extracted as the POD mode 1

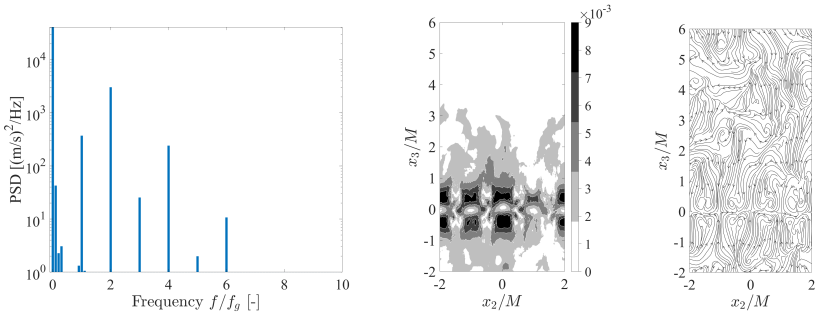

Figure 3 (a) Power spectrum density, (b) contour of velocity magnitude, and (c) streamlines for the flow structure extracted as the POD mode 2

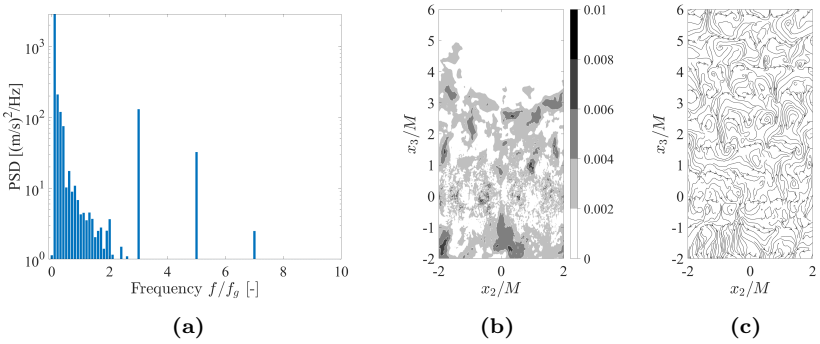

Figure 4 (a) Power spectrum density, (b) contour of velocity magnitude, and (c) streamlines for the flow structure extracted as the POD mode 5

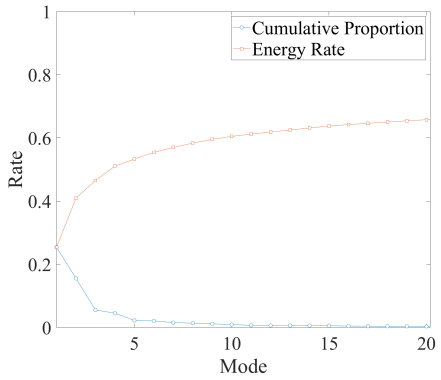

Figure 5 POD Mode energy rate and cumulative proportion

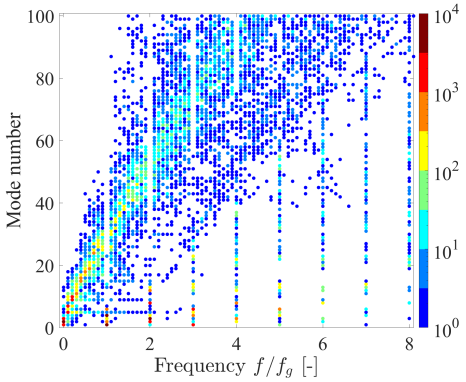

Figure 6 Power spectrum density of POD mode upto 100

velocity seems to be very small. Furthermore, from Figure 7(b), vertically stretched vortex structures having approximately one grid mesh size can be seen at both sides of the grid rod. In the region of $x_3/M > 0.5$, no distinct structures are observed. Similar to the POD analysis in the previous subsection, there are several DMD modes, having the same trend as the DMD mode 1, which capture flow structures with vortices in the vicinity of the oscillating grid and fluctuating with integer multiples of f_g. It is observed from these results that, for the dominant temporal frequency of the structure with $n \times f_g$, the number of vortices appearing on both sides of the grid rod are $2n$.

Next, the structure extracted as the DMD mode 2 (Figure 8) is discussed. This mode has a zero frequency and an amplification rate of approximately unity, which demonstrates that this mode is a stationary mode. From Figure 8(a), it is observed that, a large velocity region exists in the region of $x_3/M < 0.5$, which is similar to the DMD mode 1. However, a discrepancy can be found in the region of $x_3/M > 0.5$ where the velocity is larger than that for the DMD mode 1. From Figure 8(b), a jet-like flow structure ejecting from the space in between the grid rods is observed.

Finally, the structure extracted as the DMD mode 5 (Figure 9) is discussed. The frequencies of these modes are $0.0916 f_g$, indicating that this structure is not directly related to the oscillation of the grid. Figures 9(a) shows that the velocity decays as x_3/M becomes larger, up to $x_3/M = 4$. It is probably due to the loss of energy as the working fluid moves away from the grid. In Figures 9(b), no large-scale flow structure are evident, and instead, the mode consists only of small-scale structures. These observetions suggest that this mode primarily captures the turbulence diffusion structures. Figure 10 shows vertical profile of horizontally averaged velocity $\langle u \rangle$ for the DMD modes extracting the turbulence diffusion structures. As can be seen in this figure, the velocity is larger and maintained in the region away from the grid for the DMD mode with low fluctuating frequency. This can be attributed to the fact that the flow structures with lower frequencies often have larger energy.

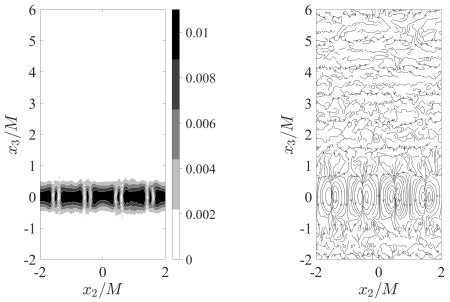

(a) **(b)**

Figure 7 (a) Contour of velocity magnitude, (b) streamlines for DMD Mode 1. Freqency : 2.0036 Hz, Growth rate : 0.99982

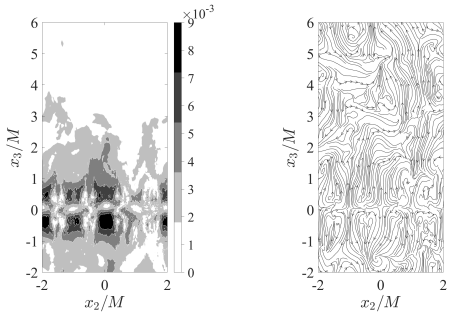

(a) **(b)**

Figure 8 (a) Contour of velocity magnitude, (b) streamlines for DMD Mode 2. Freqency : 0 Hz, Growth rate : 0.99868

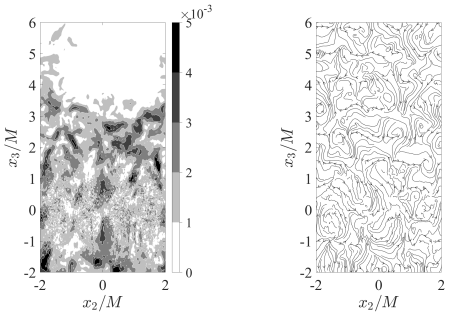

(a) **(b)**

Figure 9 (a) Contour of velocity magnitude, (b) streamlines for DMD Mode 5. Freqency : 0.1832 Hz, Growth rate : 0.99526

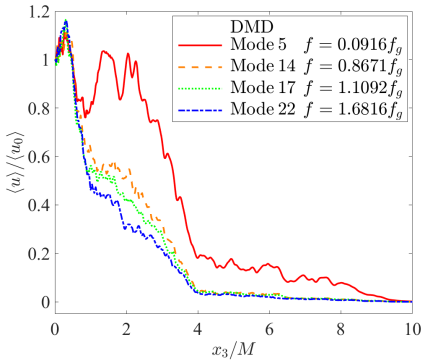

Figure 10 Profile of the horizontal velocity averaged over x_2 direction, $\langle u \rangle$, as a function of x_3. $\langle u_0 \rangle$ is the $\langle u \rangle$ value at $x_3/M = 0$.

4.3 Effects of Rotation

Distinct difference cannot be observed in the flow field between the systems at rest and with rotation. However, the effect of rotation appears in the PSD distribution for POD modes and the rank for DMD modes which is evaluated in this subsection.

First of all, the effect of rotation appearing in the POD results is discussed. Scatters of PSD for the POD modes from 1 to 100 of system with rotation is shown in Figure 11. Comparing this result with that for the system at rest (Figure 6), it can be observed that the PSD distribution for the system with rotation is more dispersed than that for the system at rest, while overall tendencies are the same as each other. Additionally, for the system with rotation, there are PSD peaks approximately at the frequency $f_g(= 2[\mathrm{Hz}])$ for the POD modes whose number is smaller than 30. Since the highly ranked POD modes describe the flow structures with large energy, it is inferred that these structures having frequencies of $n \times f_g$ (n : integer) in the system at rest are reinfoced by the rotaion. From the results shown in the previous section, it has been demonstrated that flow structures of which fluctuating frequency is not integer multiples f_g or 0 are considered to be a turbulence diffusion structure. Therefore, the contribution of the turbulence diffusion structure around the frequency f_g to flow field is increased by the system rotation.

Next, the effect of rotation appearing in the DMD results is discussed. The DMD modes, up to mode 20, ordered by the greedy algorithm are shown with their frequencies f and f/f_g in Tables 1 and 2 for the systems at rest and with rotation, respectively. For the system at rest, the DMD modes 1, 3, 4, 9, and 15 have the frequencies of integer multiples of f_g, whereas in the system with rotation the DMD modes 1, 3, 5, and 13 have similar frequences. This fact indicates that the modes having frequencies of non-integer multiples of f_g become more prioritized in the system with rotation. As discussed in the previous section, these DMD modes are considered to describe the turbulence diffusion structures. This is qualitatively consistent with our previous study [6] showing that turbulence diffusion is enhanced by the system rotation. Additionally, it is considered that the contribution of the turbulence diffusion structure around the frequency f_g to the flow field are most amplified by the rotation.

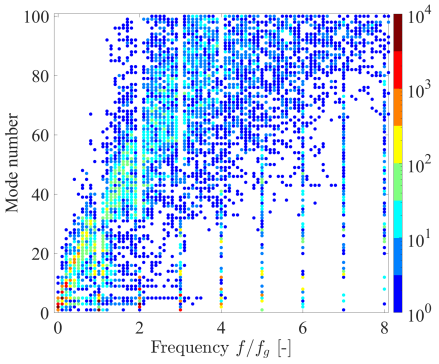

Figure 11 Power spectrum density of POD mode up to 100 in rotation system

Table 1 Frequency of DMD modes in the system at rest

Mode number	Frequency f [Hz]	f/f_g
1	2.0036	1.0018
2	0	0
3	4.0024	2.0012
4	5.9998	2.9999
5	0.1832	0.0916
6	0.3512	0.1756
7	0.5581	0.2790
8	0.7676	0.3838
9	7.9796	3.9898
10	0.9767	0.4884
11	1.1899	0.5950
12	1.5781	0.7891
13	1.3943	0.6972
14	1.7342	0.8671
15	9.9919	4.9960
16	2.3903	1.1952
17	2.2184	1.1092
18	2.5689	1.2845
19	2.7509	1.3755
20	2.9716	1.4858

Table 2 Frequency of DMD modes in the system with rotation

Mode number	Frequency f [Hz]	f/f_g
1	2.0012	1.0006
2	0	0
3	4.0019	2.0010
4	0.1722	0.0861
5	6.0114	3.0057
6	0.3824	0.1912
7	0.5982	0.2991
8	0.7519	0.3759
9	0.9473	0.4737
10	2.1604	1.0802
11	1.1563	0.5782
12	1.3626	0.6813
13	8.0310	4.0155
14	1.5747	0.7874
15	1.7815	0.8908
16	0	0
17	2.5643	1.2822
18	2.4188	1.2094
19	2.7928	1.3964
20	2.9968	1.4984

5 Conclusion

In this study, we performed the DNS of oscillating grid turbulence in the systems at rest and with rotation to investigate the effects of rotation on turbulence diffusion. Then, we applied the POD and DMD methods to the velocity field obtained by the DNS data for $Ro = 0$ and 4.77. The results of the present study are summarized as follows:

From the POD results, it was found that the flow structures were mainly categorized into following three types: 1) large vortex structures existing in the vicinity of the oscillating grid which mainly fluctuates with the frequency of f_g, 2) jet-like structures where they eject from the grid and the frequency of zero is dominant, 3) turbulent diffusion structures having the frequencies of non-integer multiples of f_g. From a result of the PSD distribution of POD modes, it was observed that some of the POD modes categorized at the turbulent diffusion structures showed a difference in PSD peaks between the systems at rest and with rotation, where an additional frequency peak at f_g is observed in the system with rotation. It can be suggested from this result that the structures are reinforced by the system rotation.

The characteristic flow structures extracted from the DMD result are found to be almost the same as those extracted from the POD results. The orders of the DMD modes for the diffusion structures become more prioritized in the system with rotation, comparing them to those in the system at rest. This is considered to be due to the reinforcement of these structures by the system rotation, which is consistent with our previous experiments.

This research is financially supported by the JSPS KAKENHI Grant Number 24K00802.

References

[1] L. Jacquin, O. Leuchter, C. Cambonxs, and J. Mathieu. Homogeneous turbulence in the presence of rotation. *Journal of Fluid Mechanics*, 220:1–52, 1990.

[2] E.J. Hopfinger, F.K. Browand, and Y. Gagne. Turbulence and waves in a rotating tank. *Journal of Fluid Mechanics*, 125:505–534, 1982.

[3] S.C. Dickinson and R.R. Long. Oscillating-grid turbulence including effects of rotation. *Journal of Fluid Mechanics*, 126:315–333, 1983.

[4] F.S. Godeferd and L. Lollini. Direct numerical simulations of turbulence with confinement and rotation. *Journal of Fluid Mechanics*, 393:257–308, 1999.

[5] Marie Poulain-Zarcos, Matthieu J Mercier, and Alexandra ter Halle. Global characterization of oscillating grid turbulence in homogeneous and two-layer fluids, and its implication for mixing at high peclet number. *Physical Review Fluids*, 7(5):054606, 2022.

[6] K. Uchida, S. Shibata, T. Yamada, and Y. Morinishi. The effect of small rotation on turbulence structure in oscillating grid turbulence. In *Proceedings of The ASME-JSME-KSME Joint Fluids Engineering Conference (AJKFED2023)*, Osaka, Japan, 4-05-1-01, July 2023.

[7] J.H. Williamson. Low-storage runge-kutta schemes. *Journal of Computational Physics*, 35(1):48–56, 1980.

[8] A.A. Amsden and F.H. Harlow. The smac method - a numerical technique for calculating incompressible fluid flows. *Los Alamos Scientific Laboratory*, 1970.

[9] T. Yamada, R. Ohno, and Y. Morinishi. Direct poisson solver combining domain decomposition and influence matrix methods and its application to DNS of oscillating grid turbulence. In *Proceedings of the Twelfth International Conference on Computational Fluid Dynamics (ICCFD12)*, Kobe, Japan, 11-A-03, July 2024.

[10] J.N. Kutz, S.L. Brunton, B.W. Brunton, and J.L. Proctor. *Dynamic mode decomposition: data-driven modeling of complex systems*. SIAM, 2016.

[11] M.R. Jovanović, P.J. Schmid, and J.W. Nichols. Sparsity-promoting dynamic mode decomposition. *Physics of Fluids*, 26(2), 2014.

[12] Y. Ohmichi. Preconditioned dynamic mode decomposition and mode selection algorithms for large datasets using incremental proper orthogonal decomposition. *AIP Advances*, 7(7), 2017.